5-2023

On the spectral density of fractional Ornstein-Uhlenbeck Process: Approximation, Estimation, and Model Comparison

Shuping SHI

Jun YU
Singapore Management University, yujun@smu.edu.sg

Chen ZHANG
Singapore Management University, chenzhang@smu.edu.sg

SMU ECONOMICS & STATISTICS

On the Spectral Density of Fractional Ornstein-Uhlenbeck Process: Approximation, Estimation, and Model Comparison

Shuping Shi, Jun Yu, Chen Zhang

May 2023

Paper No. 08-2023

On the Spectral Density of Fractional Ornstein-Uhlenbeck Process: Approximation, Estimation, and Model Comparison *

Shuping Shi†, Jun Yu††, Chen Zhang††

† Macquarie University

††Singapore Management University

May 4, 2023

Abstract

This paper introduces a novel method for accurately approximating the spectral density of the discretely-sampled fractional Ornstein-Uhlenbeck (fOU) process. We utilize this approximated spectral density to develop an estimation method called the approximated Whittle maximum likelihood method (AWML) for fOU. Additionally, we develop a likelihood-ratio (LR) test using the approximated spectral densities to distinguish between the fractional Brownian motion (fBm) and fOU processes, two popular models in the volatility literature. Simulation studies demonstrate that the AWML method improves the estimation speed and accuracy compared to existing ones and that the LR test is effective in distinguishing between the two processes when deviations are moderate. We then apply the AWML method and the LR test to the log realized volatility of 40 financial assets. Our findings reveal that the estimated Hurst parameters for these assets fall within the range of 0.10 to 0.23, indicating a rough volatility dynamic. Moreover, our LR test results suggest that both fBm and fOU are empirically relevant, with some financial assets favoring fBm and others leaning towards fOU. The proposed LR test can provide valuable guidance for selecting an appropriate model in empirical applications.

*We would like to thank Tetsuya Takabatake for helpful comments. Shuping Shi, Department of Economics, Macquarie University, Sydney, Australia. Email: shuping.shi@mq.edu.au. Jun Yu, School of Economics and Lee Kong Chian School of Business, Singapore Management University, 90 Stamford Road, Singapore 178903. Email: yujun@smu.edu.sg. Chen Zhang, School of Economics, Singapore Management University, 90 Stamford Road, Singapore 178903. Email: chenzhang@smu.edu.sg. Yu and Zhang would like to acknowledge the research support provided by the Ministry of Education, Singapore, under its Academic Research Fund (AcRF) Tier 2 (Award Number MOE-T2EP402A20-0002).

JEL classification: C12, C22, G01

Keywords: Fractional Brownian motion; fractional Ornstein-Uhlenbeck process; spectral density; Paxson approximation; Whittle likelihood; Realized volatility

1 Introduction

The fractional Ornstein-Uhlenbeck (fOU) process is a stochastic process widely employed in finance, physics, biology, and other fields to model diverse phenomena. An essential parameter of the fOU process is the Hurst exponent (H), which determines the degree of memory in the process. When $H = 0.5$, the fOU process becomes the standard Ornstein-Uhlenbeck (OU) process. For $H > 0.5$, the process is characterized by long memory, while for $H < 0.5$, the process exhibits rough dynamics. In finance, the fOU process is commonly used to model the volatility of financial assets. (See, e.g., Gatheral et al., 2018, Wang et al., 2023, Fukasawa et al., 2022, Bennedsen et al., 2022).

The spectral density is a powerful tool for analyzing the frequency characteristics of a time series. It has been utilized extensively to identify the presence of periodic patterns, trends, and cycles in the data[1] Moreover, the spectral density has proven valuable in parameter estimation (Whittle, 1954, Christiano and Vigfusson, 2003) as well as in hypothesis testing (McElroy, 2016). Unfortunately, obtaining the spectral density of discretely sampled fOU processes involves an infinite summation, which poses numerical challenges in practical applications. The commonly used truncation method can have poor accuracy when H is small (e.g., 0.1), even with a high threshold. To address this issue, we propose a novel approach to approximate the spectral density of fOU processes, inspired by the method of Paxson (1997) for fractional Gaussian noise (fGn). The proposed method, which is referred to as the Paxson approximation, leverages the monotonicity of the summand to obtain both the lower and upper bounds of the spectral density and takes the average of these bounds as an estimate of the spectral density. Compared to the truncation method, the Paxson method offers greater accuracy and computational efficiency, making it suitable for various applications.

We demonstrate the practical value of the Paxson approximate spectral density for both model estimation and hypothesis testing. Specifically, we introduce the approximate Whittle maximum likelihood (AWML) method for estimating fOU processes. This method involves replacing the spectral density of fOU with its Paxson approximation in the frequency-domain maximum likelihood (ML) approach. The asymptotic properties of AWML are identical to those of the standard Whittle ML method. Through a simulation study, we compare the finite sample performance of the AWML method with two existing methods: the maximum composite likelihood (MCL) method (Bennedsen et al., 2022) and the change-of-frequency (CoF) approach (Wang et al., 2023). The AWML method proves to be the most accurate of the three, with CoF being the least accurate. Furthermore, the AWML method is computationally more

[1] See, e.g., Burnside (1998), Messina et al. (2009), McElroy and Roy (2017), Angeletos et al. (2020).

efficient than MCL.

Next, we illustrate how the Paxson approximate spectral density can be utilized to create a likelihood ratio (LR) test that distinguishes between fOU and fractional Brownian motion (fBm) processes. Financial volatility has been modeled using both fBm and fOU processes in various studies. For instance, Gatheral et al. (2018), Wang et al. (2022), Chong et al. (2022) and Shi et al. (2022) model log volatility as an fBm process, while Bayer et al. (2016), Gatheral et al. (2018), Wang et al. (2023) and Bolko et al. (2022) utilize the fOU specification for volatility. The likelihood ratio test can shed light on the empirical relevance of these two model specifications and offer essential guidance for selecting an appropriate model in empirical applications. The LR statistic is constructed from the Paxson approximated spectral densities of the two models and the periodogram. A bootstrapping procedure is employed to obtain critical values of the LR statistic. Our simulation study reveals that the LR test has satisfactory finite sample performance.

In the empirical application, we apply the proposed estimation method for fOU and the LR test (H_0 : fBm versus H_1 : fOU) to the log realized volatility of 40 financial assets. Our estimation results suggest that volatility always exhibits rough dynamics, with the Hurst parameter ranging from 0.1 to 0.25. Our LR test results are mixed, with about half of them favoring fBm while the other half favoring fOU.

The rest of the paper is organized as follows. In Section 2, we introduce the fOU process and the spectral density of discretely sampled fOU. Section 3 derives the Paxson approximate spectral density and evaluates the approximation accuracy. Section 4 discusses how to implement the AWML method based on the Paxson approximate spectral density, its asymptotic theory, and its finite sample performance (relative to alternative estimation methods). Section 5 demonstrates the usefulness of the Paxson approximate spectral density for conducting the LR test. We present the empirical results in Section 6. The proofs are provided in the Appendix.

2 Fractional OU Process

The fOU process $\{y_t : t \in \mathbb{R}\}$ is the stochastic process given by

$$dy_t = \kappa(\mu - y_t)\,dt + \sigma dB_t^H \text{ with } y_0 = O_p(1),$$

where $\sigma > 0$, μ is a constant, and B_s^H is a fractional Brownian motion process with the Hurst parameter $H \in (0,1)$. The fBm is a Gaussian process with mean zero and autocovariance given by

$$Cov\left(B_t^H, B_s^H\right) = \frac{1}{2}\left(|t|^{2H} + |s|^{2H} - |t-s|^{2H}\right), \ \forall t,s \in (-\infty,+\infty), \tag{1}$$

It includes the standard Brownian motion (Bm) process as a special case with $H = 0.5$. Just like the Bm, the fBm is nonstationary for all $H \in (0,1)$. However, the first difference or increment of fBm, which is fGn, is always stationary. The fBm has sample paths smoother (rougher) than the standard Bm when $H > 0.5$ ($H < 0.5$). The autocovariances of fGn are not summable when $H > 0.5$ (i.e. exhibiting long memory) but sum to zero when $H < 0.5$ (i.e. exhibiting anti-persistence).

The fOU process reduces to the traditional OU process when $H = 0.5$ and to the fBm when $\kappa = 0$. When $\kappa > 0$, fOU is stationary. When $\kappa < 0$, fOU is explosive. In this paper, we assume that $\kappa > 0$. The fOU process is (locally) Hölder continuous of order $H - \varepsilon$ (Gatheral et al., 2018, Gehringer and Li, 2020). The fOU process has a unique path-wise solution:

$$y_t = e^{-\kappa t} y_0 + \left(1 - e^{-\kappa t}\right) \mu + \int_{-\infty}^{t} \sigma e^{-\kappa(t-u)} dB_u^H, \tag{2}$$

where $E(y_t) = \mu$ and $Var(y_t) = \sigma^2 \kappa^{-2H} H \Gamma(2H)$ with $\Gamma(.)$ being the Gamma function. See Hu and Nualart (2010). When $\kappa > 0$, the autocovariance of fOU is given by

$$\gamma_k = \frac{\sigma^2}{2\kappa^{2H}} \left(\frac{1}{2} \int_{-\infty}^{\infty} e^{-|s|} \left|\kappa k + s\right|^{2H} ds - \left|\kappa k\right|^{2H} \right). \tag{3}$$

and its spectral density is

$$f_y(\lambda) = \frac{\sigma^2}{2\pi} C(H) \left|\lambda\right|^{1-2H} (\kappa^2 + \lambda^2)^{-1} \text{ for } \lambda \in (-\infty, \infty), \tag{4}$$

where $C(H) = \Gamma(2H+1)\sin(\pi H)$. See Garnier and Sølna (2018) for the autocovariance and Hult (2003) for the spectral density.

Empirical observations are often sampled at a fixed sampling interval (denoted by Δ). The discrete-time observations from the fOU process are denoted by $\left\{y_{j\Delta}\right\}_{j=1}^{n}$, where n is the total number of observations. Hence, $T = n\Delta$ is the time span. The spectral density of discretely-sampled fOU is provided by Hult (2003) and takes the form of

$$f_y^{\Delta}(\lambda) = \frac{\sigma^2}{2\pi} C(H) \Delta^{2H} \sum_{k=-\infty}^{\infty} \frac{\left|\lambda + 2\pi k\right|^{1-2H}}{(\kappa\Delta)^2 + (\lambda + 2\pi k)^2} \text{ for } \lambda \in [-\pi, \pi]. \tag{5}$$

3 Paxson Approximation of Spectral Density

We now derive the Paxson approximate spectral density for discretely-sampled fOU. The discretely-sampled spectral density of fOU (5) involves the infinite sum

$$S(\lambda) \equiv \sum_{k=-\infty}^{\infty} \frac{|\lambda + 2\pi k|^{1-2H}}{(\kappa\Delta)^2 + (\lambda + 2\pi k)^2},$$

which can be rewritten as

$$\begin{aligned} S(\lambda) &= \sum_{k=-\infty}^{-1} \frac{(-\lambda - 2\pi k)^{1-2H}}{(\Delta\kappa)^2 + (\lambda + 2\pi k)^2} + \frac{\lambda^{1-2H}}{(\Delta\kappa)^2 + \lambda^2} + \sum_{k=1}^{\infty} \frac{(\lambda + 2\pi k)^{1-2H}}{(\Delta\kappa)^2 + (\lambda + 2\pi k)^2} \\ &= \sum_{k=1}^{\infty} \frac{(2\pi k - \lambda)^{1-2H}}{(\Delta\kappa)^2 + (2\pi k - \lambda)^2} + \frac{\lambda^{1-2H}}{(\Delta\kappa)^2 + \lambda^2} + \sum_{k=1}^{\infty} \frac{(\lambda + 2\pi k)^{1-2H}}{(\Delta\kappa)^2 + (\lambda + 2\pi k)^2} \\ &\equiv \sum_{k=1}^{\infty} Q(k) + Q_0 + \sum_{k=1}^{\infty} \tilde{Q}(k), \end{aligned}$$

where $Q(k) \equiv \frac{(2\pi k - \lambda)^{1-2H}}{(\Delta\kappa)^2 + (2\pi k - \lambda)^2}$ and $\tilde{Q}(k) \equiv \frac{(\lambda + 2\pi k)^{1-2H}}{(\Delta\kappa)^2 + (\lambda + 2\pi k)^2}$. Some theoretical properties of $Q(k)$ and $\tilde{Q}(k)$ are provided in Lemma 3.1.

Lemma 3.1 *(1) The quantity $Q(k)$ is monotonically decreasing when $k > \frac{\Delta\kappa + \lambda}{2\pi}$; (2) The quantity $\tilde{Q}(k)$ is monotonically decreasing when $k > \frac{\Delta\kappa - \lambda}{2\pi}$; (3) For $K > \frac{\Delta\kappa + \lambda}{2\pi}$,*

$$\begin{aligned} a(K,H,\lambda) &\leq \sum_{x=K+1}^{\infty} Q(k) \leq \frac{1}{4\pi H} (2\pi K - \lambda)^{-2H}, \\ b(K,H,\lambda) &\leq \sum_{x=K+1}^{\infty} \tilde{Q}(k) \leq \frac{1}{4\pi H} (2\pi K + \lambda)^{-2H}, \end{aligned}$$

where

$$a(K,H,\lambda) \equiv \frac{1}{4\pi} [2\pi(K+1) - \lambda]^{-2H} \left\{ \frac{1}{H} - \frac{(\Delta\kappa)^2}{(1+H)[2\pi(K+1) - \lambda]^2} \right\}, \tag{6}$$

$$b(K,H,\lambda) \equiv \frac{1}{4\pi} [2\pi(K+1) + \lambda]^{-2H} \left\{ \frac{1}{H} - \frac{(\Delta\kappa)^2}{(1+H)[2\pi(K+1) + \lambda]^2} \right\}. \tag{7}$$

Lemma 3.1 implies that both $Q(k)$ and $\tilde{Q}(k)$ are monotonically decreasing when $k > (\Delta\kappa + \lambda)/(2\pi)$. This requirement is not at all restrictive. For example, if we assume that $\lambda = \pi$ (upper bound) and $\kappa\Delta = 10$ (a very large value in the empirical sense), the threshold is only 2.09. The monotonicity of $Q(k)$ and $\tilde{Q}(k)$ is crucial to the derivation of the results in Lemma 3.1(3). See Appendix A for details.

By applying Lemma 3.1(3), we can derive both the lower and upper bounds for the spectral densities, which are presented in (17) in the Appendix. The Paxson approximation is then obtained as the average of these two bounds. The analytical expressions for the Paxson approximation are given in Theorem 3.1, with its proof in Appendix A.

Theorem 3.1 *The Paxson approximation of the spectral density of discretely-sampled fOU is*

$$f_y^{\Delta}(\lambda) \approx \hat{f}_y^{\Delta}(\lambda) \equiv \frac{\sigma^2}{2\pi} C(H) \Delta^{2H} \left[\sum_{k=1}^{K} Q(k) + \sum_{k=1}^{K} \tilde{Q}(k) + \frac{\lambda^{1-2H}}{(\Delta\kappa)^2 + \lambda^2} + \frac{1}{2} a(K,H,\lambda) + \frac{1}{2} b(K,H,\lambda) + c(K,H,\lambda) \right], \tag{8}$$

where $K > \frac{\Delta\kappa+\lambda}{2\pi}$, $C(H) = \Gamma(2H+1)\sin(\pi H)$, *and*

$$c(K,H,\lambda) \equiv \frac{1}{8\pi H}(2\pi K - \lambda)^{-2H} + \frac{1}{8\pi H}(2\pi K + \lambda)^{-2H}.$$

Approximation Accuracy

We evaluate the accuracy of two methods for approximating the spectral density (5): the truncation method and the Paxson method. The truncation method is commonly used in practice, where the infinite sum $\sum_{k=-\infty}^{\infty}$ is replaced by $\sum_{k=-K}^{K}$. We consider various settings of the model parameters with a constant sampling interval of $\Delta = 1/250$, which corresponds to daily observations over a one-year period. Specifically, we consider three values of the Hurst parameter ($H = 0.1, 0.2, 0.7$) and two values of the mean-reverting parameter ($\kappa = 25, 250$). Based on the path-wise solution (2), we may obtain the exact discrete time representation of fOU as:

$$y_{j\Delta} = e^{-\kappa\Delta} y_{(j-1)\Delta} + \left(1 - e^{-\kappa\Delta}\right)\mu + \varepsilon_{j\Delta} \text{ with } \varepsilon_{j\Delta} = \sigma \int_{(j-1)\Delta}^{j\Delta} e^{-\kappa(j\Delta - u)} dB_u^H.$$

The values of κ and Δ imply that the autoregressive coefficient is approximately 0.90 and 0.37 for $\kappa = 25$ and $\kappa = 250$, respectively.

Figure 1 corresponds to the case where $\kappa = 25$, while Figure 2 corresponds to $\kappa = 250$. The first row of both figures displays the Paxson approximation (9) (with $K = 200$) and the lower and upper bounds of the spectral densities obtained from (17). The x-axis is the spectral frequency λ ranging from 0 to π. The y-axis corresponds to the spectral density $f_y^{\Delta}(\lambda)$. It is evident that the three lines are nearly indistinguishable under all parameter settings, suggesting that the Paxson approximation errors are negligible.

The second row of the figures compares the accuracy of the Paxson approximation with that of the truncation method, which uses thresholds of $K = 2000, 5000, 20000$. We observe that the truncation

Figure 1: Approximation spectral densities: $\kappa = 25$ and $\Delta = 1/250$ (i.e. $e^{-\kappa\Delta} \approx 0.90$))

(a) Paxson: $H = 0.1$ (b) Paxson: $H = 0.2$ (c) Paxson: $H = 0.7$

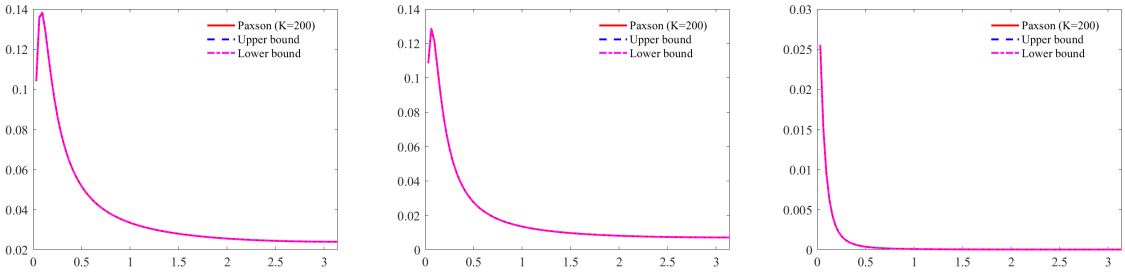

(d) Paxson v.s. truncation: $H = 0.1$ (e) Paxson v.s. truncation: $H = 0.2$ (f) Paxson v.s truncation: $H = 0.7$

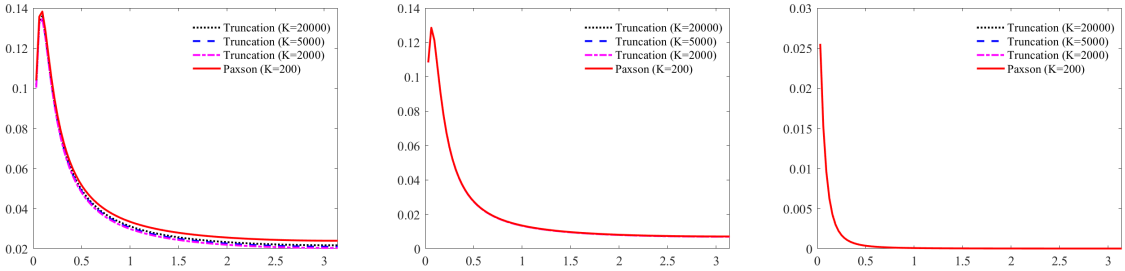

Note: The x-axis is the spectral frequency λ ranging from zero to π and the y-axis is the approximate spectral density, which is computed from (9) for Paxson and (5) for the truncation method. The lower and upper bounds of $f_y^{\Delta}(\lambda)$ are computed from (17) in the Appendix.

method performs well for some parameter settings but not all. Specifically, the approximation accuracy is poor when H is close to zero or when $e^{-\kappa\Delta}$ is small. This observation is consistent with equation (5). When the value of K is sufficiently large so that the summand in (5) monotonically decreases for $k > K$, the summand itself declines more slowly as H approaches zero. Furthermore, for a given value of H, a larger $\kappa\Delta$ is associated with a slower rate of decline in the summand. Therefore, to achieve an accurate approximation, a larger truncation order K is required when H is smaller or when $\kappa\Delta$ is larger. As we can see from the graphs, the spectral density of the truncation method approaches the Paxson approximation as the truncation order K increases. However, even with $K = 20000$, the approximation error remains significant for $H = 0.1$ and $\kappa\Delta = 1$ in Figure 2. It is important to note that the truncation method becomes computationally intensive when the truncation order K is large.

4 Application I: Model Estimation

In this section, we introduce the approximate Whittle maximum likelihood (AWML) method for estimating the Hurst parameter of the fOU process, based on the Paxson approximate spectral density. We compare the performance of AWML with two existing methods: the MCL approach and the CoF ap-

Figure 2: Approximate spectral densities: $\kappa = 250$ and $\Delta = 1/250$ (i.e. $e^{-\kappa\Delta} \approx 0.37$)

(a) Paxson: $H = 0.1$ (b) Paxson: $H = 0.2$ (c) Paxson: $H = 0.7$

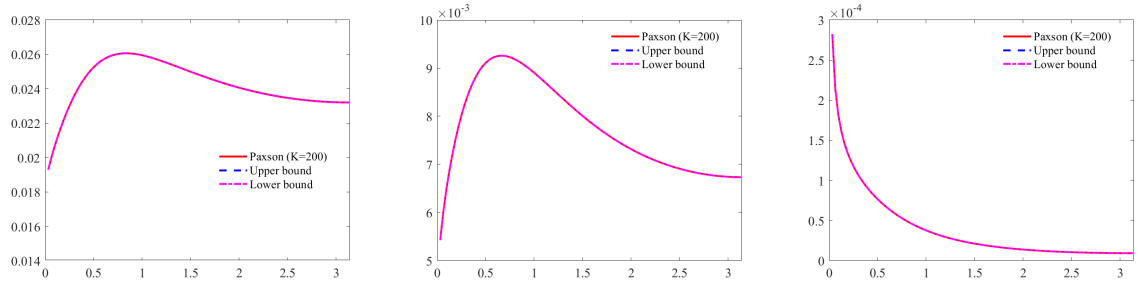

(d) Paxson v.s. truncation: $H = 0.1$ (e) Paxson v.s. truncation: $H = 0.2$ (f) Paxson v.s. truncation: $H = 0.7$

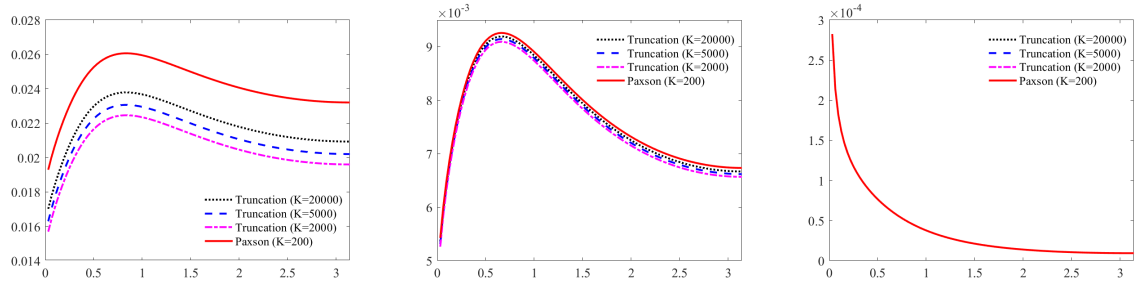

Note: The x-axis is the spectral frequency λ ranging from zero to π and the y-axis is the approximate spectral density, which is computed from (9) for Paxson and (5) for the truncation method. The lower and upper bounds of $f_x^{\Delta}(\lambda)$ are computed from (17) in the Appendix.

proach. Our main focus is on the Hurst parameter, which is a key parameter in the fOU process. We demonstrate that AWML provides an effective and efficient alternative to existing methods for estimating this parameter. Note that Fukasawa and Takabatake (2019) use the Paxson approximate spectral density to construct the AWML estimate of H in fGn.

4.1 Approximate Whittle ML method

Let $\{y_{j\Delta}\}_{j=1}^{n}$ be the data series of interest and $f_y^{\Delta}(\lambda) = \sigma^2 \eta(\lambda;\beta)$ be its spectral density with β containing all parameters except σ. Let $Z = \exp\left(-\frac{1}{2\pi}\int_{-\pi}^{\pi} \log \eta(\lambda;\beta) d\lambda\right)$ and $\tilde{f}_y^{\Delta}(\lambda) = \sigma^2 \tilde{\eta}(\lambda;\beta)$ be the normalized spectral density with $\tilde{\eta}(\lambda;\beta) = \eta(\lambda;\beta)Z$. The normalized spectral density satisfies the property that

$$\int_{-\pi}^{\pi} \log \tilde{\eta}(\lambda;\beta)\, d\lambda = 0. \tag{9}$$

The log Whittle likelihood function (Whittle, 1951) is specified as

$$\log L_W(\beta) = \frac{1}{m}\sum_{s=1}^{m} \frac{I(\lambda_s)}{\tilde{\eta}(\lambda_s;\beta)}, \tag{10}$$

where $m = \lfloor n/2 \rfloor$, $\lambda_s = 2\pi s/n$ with $s = 1, ..., m$ and $I(\lambda_s)$ is the periodogram at the s^{th} Fourier frequency λ_s defined as

$$I(\lambda_s) = \frac{1}{2\pi n} \left| \sum_{j=1}^{n} z_j \exp(-ij\lambda_s) \right|^2. \tag{11}$$

The objective function of the Whittle method (10) is derived from the time-domain ML with the approximations $\Sigma_z^{-1} \approx \left[a_{jk}\right]_{j,k=1}^{T}$, where

$$a_{jk} \approx (2\pi)^{-2} \int_{-\pi}^{\pi} f(\lambda;\theta)^{-1} e^{i(j-k)\lambda} \, \mathrm{d}\lambda \quad \text{and} \quad \log|\Sigma_z| \approx T(2\pi)^{-1} \int_{-\pi}^{\pi} \log f(\lambda;\theta) \, \mathrm{d}\lambda.$$

For the latter, replacing $f_y^{\Delta}(\lambda)$ with $\sigma^2 \tilde{\eta}(\lambda;\beta)/Z$ and using the properties of $\tilde{\eta}(\lambda;\beta)$ in (9),

$$\log|\Sigma_z| \approx T \log \sigma^2/Z + T(2\pi)^{-1} \int_{-\pi}^{\pi} \log \tilde{\eta}(\lambda;\beta) \, \mathrm{d}\lambda = T \log \sigma^2/Z,$$

which is independent of β and hence removed from the objective function, leading to (10).

The Whittle ML estimator is denoted by $\hat{\beta}_W$ and defined as

$$\hat{\beta}_W = \arg\min_{\beta} \log L_W(\beta)$$

and the parameter σ^2 is estimated separately as the sample average of the ratio between $I(\lambda_s)$ and the original spectral density $\eta(\lambda_s;\hat{\beta}_W)$, i.e.,

$$\hat{\sigma}_W^2 = \frac{1}{m} \sum_{s=1}^{m} \frac{I(\lambda_s)}{\eta(\lambda_s;\hat{\beta}_W)}.$$

The approximate Whittle ML method is expected to much more computational efficient, comparing with the time-domain ML (TDML) method, especially when the dimension n is large. This is because the implementation of the TDML method requires computing the variance covariance matrix Σ_z and its determinant and inverse (i.e., $|\Sigma_z|$ and Σ_z^{-1}), which do not have closed-form expressions.

Like the TDML method, the Whittle ML estimator is shown to be consistent, asymptotic normal and efficient in the sense of Fisher by Fox and Taqqu (1986) for strongly dependent processes whose spectral density satisfies the condition $f_y(\lambda) \sim |\lambda|^{-2d} L_\beta(\lambda)$ as $\lambda \to 0$, where $d \in (0, 1/2)$ and $L_\beta(\lambda)$ varies slowly at 0. The asymptotic results are extended to a model specification including not only rough but also non-stationary processes, i.e., $d \in (-1/2, 0)$ and $d \in [0.5, 1)$, by Velasco and Robinson (2000).[2] Note that the spectral density of fOU is $|\lambda|^{1-2H} L_\beta(\lambda)$ when $\lambda \to 0$ with $H = d + 1/2$. Since $H \in (0,1)$ is equivalent to $d \in (-1/2, 1/2)$, the asymptotic theory of Velasco and Robinson (2000) is applicable to

[2] In the case of non-stationarity, tapering should be employed.

fOU, which is stated below.

Under Assumptions A.1-A.5 and A.7-A.9 in Velasco and Robinson (2000), the standard Whittle ML estimator for fOU is consistent and has asymptotic normality:

$$\sqrt{m}\left(\hat{\beta}-\beta_0\right) \to_d N\left(0, 4\pi\Sigma_0^{-1}\right),$$

where β_0 is the true model parameter and

$$\Sigma_0 = \int_{-\pi}^{\pi} \left\{\frac{\partial}{\partial\beta}\log\eta\left(\lambda;\beta_0\right)\right\}\left\{\frac{\partial}{\partial\beta'}\log\eta\left(\lambda;\beta\right)\right\} d\lambda.$$

Moreover, $\hat{\sigma}_W^2 \to_p \hat{\sigma}^2$.

Calculating the spectral density is a crucial component in implementing Whittle ML methods, but the spectral densities of fGn and fOU involve infinite summations, making the computation of the exact spectral density challenging. As mentioned in Section 3, the truncation method is computationally demanding and inaccurate in some cases. Therefore, we propose using the Paxson approximate spectral density $\hat{f}_y^{\Delta}(\lambda)$ to replace the actual spectral density $f_y^{\Delta}(\lambda)$, resulting in an approximate Whittle ML method. The AWML estimator is denoted by $\hat{\theta}_{AW} = \left(\hat{\beta}_{AW}, \hat{\sigma}_{AW}\right)$.

4.2 Other estimation methods

We introduce the MCL method of Bennedsen et al. (2022) and the CoF method Wang et al. (2023) for fOU. Both methods are designed to improve the computational speed of TDML.

4.2.1 TDML and MCL

Let $y = (y_{1\Delta}, y_{2\Delta}, \cdots, y_{n\Delta})'$, $\theta = (H, \kappa, \sigma)$, and Σ_y be the covariance matrix of y. Since $y \sim N(0, \Sigma_y)$, the log likelihood function of fOU is

$$\log L(\theta) \propto -\frac{1}{2}\log|\Sigma_y| - \frac{1}{2}y'\Sigma_y^{-1}y. \tag{12}$$

The TDML estimator is defined as

$$\hat{\theta}_{ML} = \arg\max_{\theta} \log L(\theta).$$

The asymptotic theory of $\hat{\theta}_{ML}$ was studied in Dahlhaus (1989) when $H \in (0.5, 1)$ and Lieberman et al. (2012) when $H \in (0, 0.5)$. Under both settings, the TDML estimator is consistent, asymptotically normal, and efficient in the sense of Fisher.

However, the TDML method can be computationally intensive, which makes it unsuitable for a sample with a large sample size. To address this issue, Bennedsen et al. (2022) propose the maximum

composite likelihood method, which aims to improve the computational speed. The objective function of the MCL is given by:

$$\log L^c(\theta) = \sum_{k=1}^{K} \sum_{i=1}^{n-k} \log \omega \left(y_{(i+k)\Delta}, y_{i\Delta}; \theta \right),$$

where $K \in \mathbb{N}^+$ is fixed, $\omega \left(y_{(i+k)\Delta}, y_{i\Delta}; \theta \right)$ is the pairwise joint probability density function (pdf) of $\left(y_{(i+k)\Delta}, y_{i\Delta} \right)$. Since $\left(y_{(i+k)\Delta}, y_{i\Delta} \right)$ follows a bivariate normal distribution with correlation coefficient ρ_k, the pdf of $\left(y_{(i+k)\Delta}, y_{i\Delta} \right)$ takes the form of

$$\omega \left(y_{(i+k)\Delta}, y_{i\Delta}; \theta \right) = \frac{1}{2\pi\sigma^2 \sqrt{1-\rho_k^2}} \exp \left[-\frac{1}{2\sigma^2 \left(1-\rho_k^2\right)} \left(y_{(i+k)\Delta}^2 + y_{i\Delta}^2 - 2 y_{i\Delta} y_{(i+k)\Delta} \rho_k \right) \right].$$

The computation of the correlation coefficient ρ_k is based on formula (3) in which the indefinite integral is computed using the numerical integral evaluation function *quadgk* in Matlab. The composite maximum likelihood estimator is defined as

$$\hat{\theta}_{MCL} = \arg\max_{\theta \in \Theta} \log L^c(\theta).$$

When $H \leq 0.5$, the MCL method is shown to be consistent and asymptotically normal, with its variance depending on the range of H (Bennedsen et al., 2022).

4.2.2 CoF method

The CoF approach only relies on the first two moments of $y_{i\Delta}$ which makes it very easy to implement. The Hurst parameter H is estimated as

$$\hat{H}_{CoF} = \frac{1}{2} \log_2 \left(\frac{\sum_{j=1}^{n-4} \left(y_{(j+4)\Delta} - 2 y_{(j+2)\Delta} + y_{j\Delta} \right)^2}{\sum_{j=1}^{n-2} \left(y_{(j+2)\Delta} - 2 y_{(j+1)\Delta} + y_{j\Delta} \right)^2} \right),$$

where $\log_2$ is 2-based logarithm. The numerator and the denominator are the second order difference of $y_{j\Delta}$ at different frequencies and hence the name of the method. The remaining two parameters σ and κ are estimated in a second stage such that

$$\hat{\sigma} = \sqrt{\frac{\sum_{j=1}^{n-2} \left(y_{(j+2)\Delta} - 2 y_{(j+1)\Delta} + y_{j\Delta} \right)^2}{n \left(4 - 2^{2\hat{H}} \right) \Delta^{2\hat{H}}}} \quad \text{and} \quad \hat{\kappa} = \left(\frac{n \sum_{j=1}^{n} y_{j\Delta}^2 - \left(\sum_{j=1}^{n} y_{j\Delta} \right)^2}{n^2 \hat{\sigma}^2 \hat{H} \Gamma \left(2\hat{H} \right)} \right)^{-\frac{1}{2\hat{H}}}.$$

Both $\hat{H}$ and $\hat{\sigma}$ are consistent and asymptotically normal when $T\Delta \to 0$ and $n = T/\Delta \to \infty$. While $\hat{H}$ is $\sqrt{n}$-consistent, the convergent rate of $\hat{\sigma}$ is slower (i.e., $\sqrt{n}/\left(\log\left(1/\Delta\right)\right)$). The consistent of $\hat{\kappa}$ requires $T \to \infty$ and $\Delta \to 0$. The rate of convergence is $\sqrt{T}$ and the estimator is asymptotically normal.

4.3 Simulation study

The data generating process is fOU (2) with two parameter settings: $\{H, \kappa, \sigma^2\} = \{0.1, 1, 0.2\}$ and $\{H, \kappa, \sigma^2\} = \{0.2, 5, 1\}$, which are close to the estimated coefficients in the empirical application. We set the sample size to $n = 2,000, 4,000$ and conduct $1,000$ replications to compare the estimation accuracy of AWML, MCL, and CoF. For AWML, we use $K = 200$ for the Paxson's approximation of the spectral density as in Figures 1 and 2. We use the CoF estimate as an initial value for the numerical optimization conducted with the *fminsearch* function in Matlab.

Figure 3: Kernel densities of the estimated model parameters: $H = 0.1, \kappa = 1, \sigma^2 = 0.2$

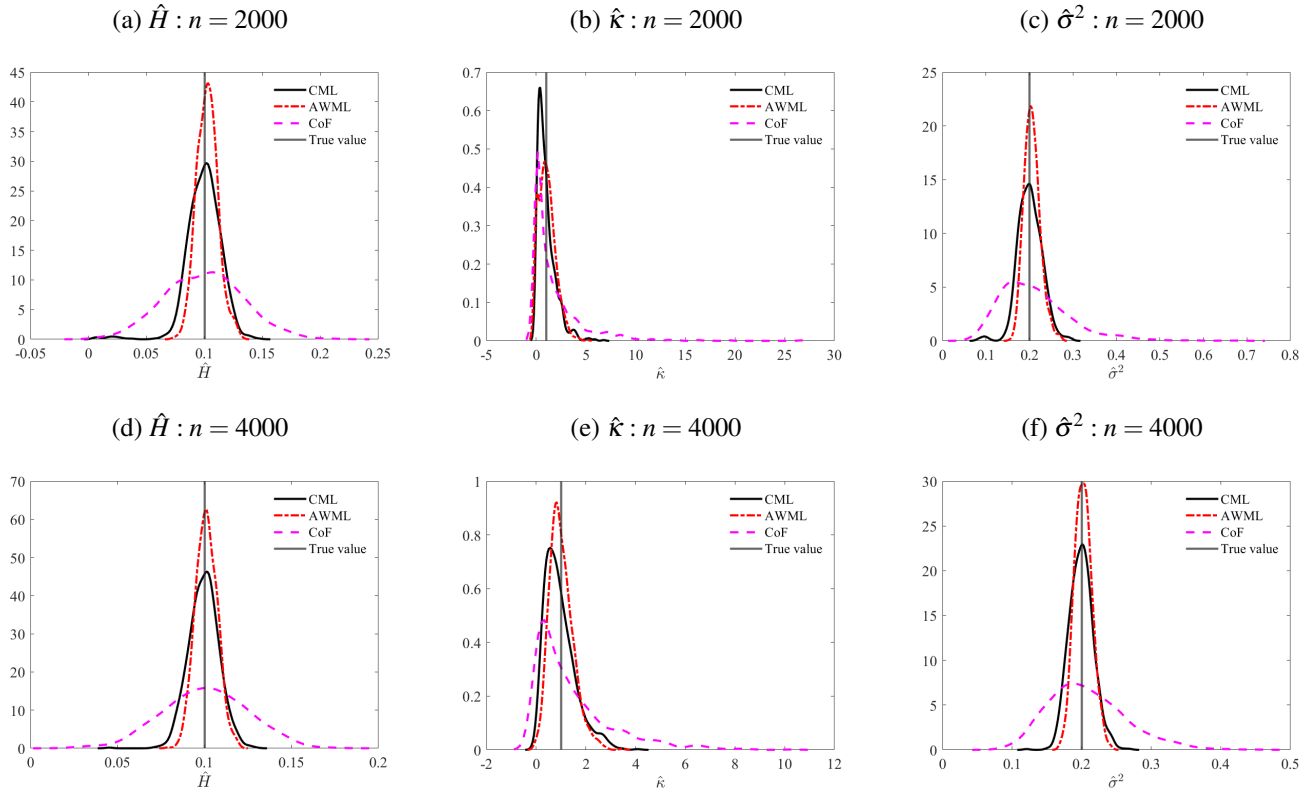

Note: The kernel densities are computed from the 1000 estimates of the model parameters. The x-axis is the estimated coefficients and y-axis displays the kernel density.

Figures 3 and 4 depict kernel density estimates of the parameter estimates from the three estimation methods for the two sets of model parameters. The top row corresponds to a sample size of $n = 2000$, while the bottom row corresponds to $n = 4000$. In terms of both bias and variance, the AWML method provides the most accurate estimation results, followed by MCL. The advantage of AWML is more pronounced in Figure 3 (with a smaller value of H) than in Figure 4. While the CoF method is computationally efficient, the estimation accuracy comes at a cost, and the distributions of CoF estimates are the most dispersed. Furthermore, the AWML method is computationally less expensive than MCL. On a standard laptop computer, it takes AWML and MCL, respectively, approximately 1.19 and 4.32 seconds

Figure 4: Kernel densities of the model parameter estimates: $H = 0.2, \kappa = 5, \sigma^2 = 1$

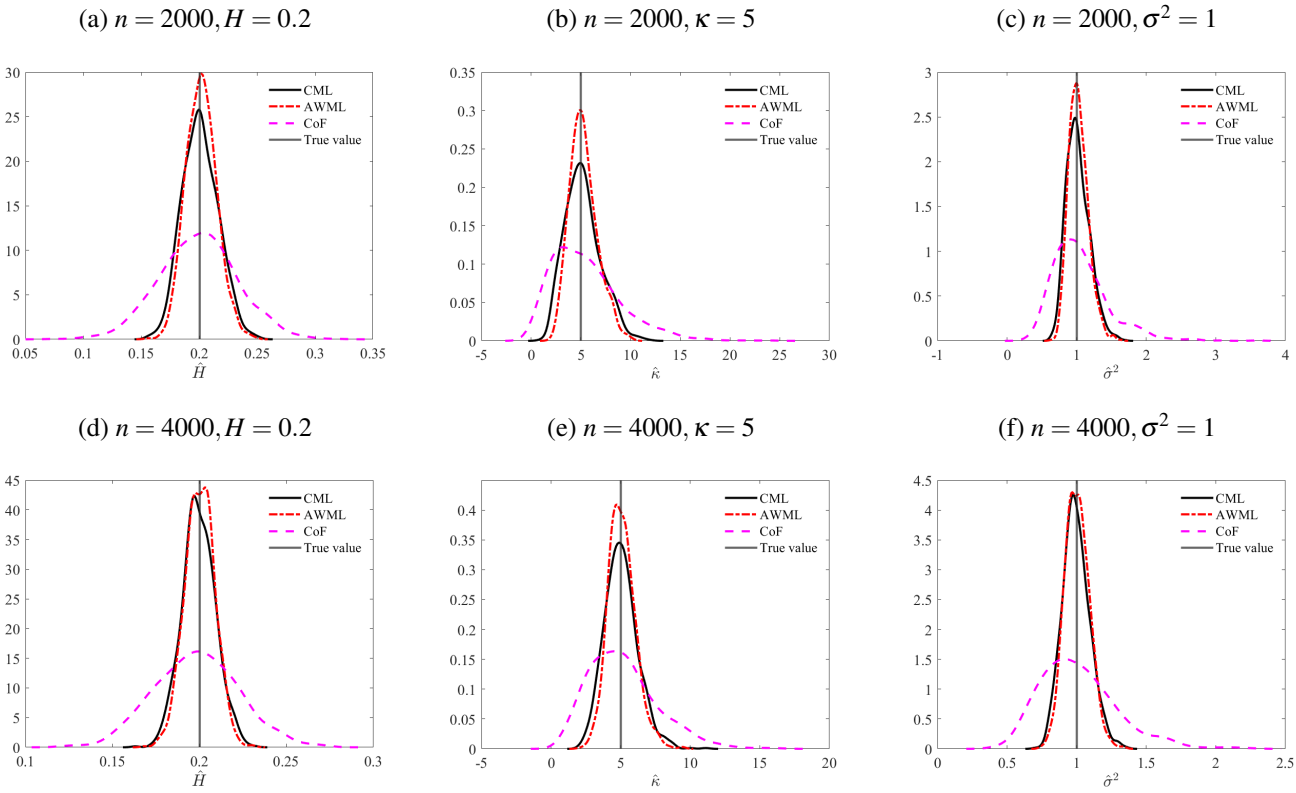

Note: The kernel densities are computed from the 1000 estimates of the model parameters. The x-axis is the estimated coefficients and y-axis displays the kernel density.

to complete one iteration.[3]

5 Application II: Hypothesis Testing

In this section, we demonstrate how the Paxson approximate spectral density facilitates the implementation of a likelihood ratio test that compares fBm (the null) with fOU (the alternative). The fBm and fOU models have gained popularity in recent volatility literature due to their ability to fit volatility surface, capture volatility dynamics, and provide accurate forecasts (see, e.g., Gatheral et al., 2018, Wang et al., 2023). The fOU process nests fBm as a special case with $\kappa = 0$.[4] Despite their widespread use, it remains an open question as to which of these models holds greater empirically relevance. The proposed likelihood ratio test can offer insight into this intriguing empirical question and provide guidance for further theoretical and empirical research.

[3]The CPU time is based on MacBook Pro M2 chip, 8-core CPU and 10-core GPU.

[4]Proposition 3.1 in Gatheral et al. (2018) gives a condition on κ under which fOU behaves locally as fBm. This condition can be easily tested using our approach.

Since fBm is a non-stationary process and LR tests are only applicable to stationary processes, we apply to the LR test on first differenced data and compare fGn (increment of fBm) against dfOU (increment of fOU) instead. Define the first difference of the process as $x_{j\Delta} = y_{j\Delta} - y_{(j-1)\Delta}$, which is a fGn when $\kappa = 0$ and dfOU when $\kappa \neq 0$. The following theorem gives the expression of the spectral density of the dfOU process.

Theorem 5.1 *The spectral density of the dfOU process is*

$$f_x^{\Delta}(\lambda) = 2(1-\cos\lambda) f_y^{\Delta}(\lambda), \text{ for } \lambda \in [-\pi, \pi] \tag{13}$$

and the Paxson approximation of the spectral density of discretely-sampled dfOU is

$$f_x^{\Delta}(\lambda) \approx \hat{f}_x^{\Delta} \equiv (\lambda)\, 2(1-\cos\lambda) \hat{f}_y^{\Delta}(\lambda). \tag{14}$$

The proof of Theorem 5.1 can be found in the Appendix. It is worth noting that the dfOU process reduces to fGn when $\kappa = 0$. The spectral density and Paxson approximate spectral density of fGn can be obtained by substituting $\kappa = 0$ into (13) and (14), respectively. The spectral density of fGn is also presented in Proposition 2.1 of Beran (1994). With this information in hand, we can now introduce the spectral density-based likelihood ratio test.

5.1 Likelihood ratio test

Consider two models of interest: $\mathscr{F}_0 = \{f_\phi : \phi \in \Theta_1\}$ and $\mathscr{F}_1 = \{f_\theta : \theta \in \Theta_2\}$ with $\phi = (H, \sigma)$ for fGn and $\theta = (H, \kappa, \sigma)$ for dfOU. These two models are nested, i.e., $\mathscr{F}_0 \subset \mathscr{F}_1$. We define the 'distance' between a given model spectral density f_ϑ and a target or true spectral f^* by

$$\mathscr{D}(f_\vartheta, f^*) = \frac{1}{m}\sum_{s=1}^{m} \log f_\vartheta(\lambda_s) + \frac{1}{m}\sum_{s=1}^{m} \frac{f^*(\lambda_s)}{f_\vartheta(\lambda_s)}.$$

The Whittle ML estimators of the two models are, respectively,

$$\hat{\phi}(I) = \arg\max_{\phi} \mathscr{D}\left(f_\phi, I\right) \text{ and } \hat{\theta}(I) = \arg\max_{\theta} \mathscr{D}(f_\theta, I),$$

where I is the periodogram specified in (11).[5] Again, we use the Paxson approximate spectral densities to replace the true ones for dfOU and fGn since the true spectral densities involve an infinite sum. The Paxson approximate spectral density of dfOU is provided in Theorem 5.1 with that of fGn being a special case of dfOU with $\kappa = 0$.

[5] This objective function formulation is equivalent to the one presented in Section 4.1 that utilizes a normalized spectral density. For estimation of these two models, we will be following the procedure described in Section 4.1.

Under the null hypothesis, $\kappa = 0$ such that the two models $\mathscr{F}_0$ and $\mathscr{F}_1$ are equidistant to the true model with respect to $\mathscr{D}$ (a.k.a divergence equivalence) given by

$$\mathscr{H}_0 : \mathscr{D}\left(f_{\hat{\phi}(f^*)}, f^*\right) = \mathscr{D}\left(f_{\hat{\theta}(f^*)}, f^*\right). \tag{15}$$

The likelihood ratio statistic is constructed as the difference between model distances to the periodogram:

$$LR = \mathscr{D}\left(f_{\hat{\phi}(I)}, I\right) - \mathscr{D}\left(f_{\hat{\theta}(I)}, I\right). \tag{16}$$

The definition of divergence equivalence and the LR statistic are discrete-time correspondence of the continuous-time version provided by McElroy (2016). Since $\frac{1}{n} y' \Sigma_y^{-1} y \approx \frac{1}{2\pi} \int_{-\pi}^{\pi} I(\lambda) f_\theta(\lambda)^{-1} d\lambda$ and $\frac{1}{n} \log|\Sigma_y| \approx \frac{1}{2\pi} \int_{-\pi}^{\pi} \log f_\theta(\lambda) d\lambda$, we have

$$\log L(\theta) = -\frac{1}{2} \log|\Sigma_y| - \frac{1}{2} y' \Sigma_y^{-1} y \approx -\frac{n}{2} \mathscr{D}(f_\theta, I)$$

and the time domain likelihood ratio statistic $\widetilde{LR}$ equals nLR, i.e.,

$$\widetilde{LR} = -2\left[\log L(\phi) - \log L(\theta)\right] = nLR.$$

According to McElroy (2016), the nLR statistic approaches a Chi-square distribution as n tends towards infinity under some regularity conditions. However, it requires the spectral density to be Lipschitz of degree $\alpha > 1/2$. This condition is, unfortunately, not satisfied by dfOU.[6] Therefore, the limiting distribution of $\widetilde{LR}$ in the current setting remains unknown. To perform statistical inference, we employ a bootstrapping procedure, the implementation of which is detailed below. We reject the null model $\mathscr{F}_0$ in favor of $\mathscr{F}_1$ if nLR exceeds the bootstrapped critical value.

Step 1: Estimate $\hat{H}$ and $\hat{\sigma}$ under the null hypothesis that $x_{j\Delta} = y_{j\Delta} - y_{(j-1)\Delta}$ follows a fractional Gaussian process using the approximate Whittle ML method.

Step 2: Simulate data $x_{j\Delta}^{(b)} \sim fGn\left(\hat{H}, \hat{\sigma}\right)$ with $j = 1, \ldots, n$.

Step 3: Compute the likelihood ratio statistic $\widetilde{LR}^{(b)}$ from $\left\{x_{j\Delta}^{(b)}\right\}_{j=1}^{n}$.

Step 4: Repeat Step 2-3 for $B = 999$ times and obtain $\left\{\widetilde{LR}^{(b)}\right\}_{b=1}^{B}$.

Step 5: The 95^{th} percentile is taken as the bootstrapped critical value of the $\widetilde{LR}$ statistic.

[6] As $\lambda \to 0$, the spectral density of the dfOU process is approximately $|\lambda|^{-2d} L_\beta(\lambda)$, where $d = H - 3/2 \in (-3/2, -1/2)$. Note that the TDML estimator for non-invertible processes ($d \leq -1/2$) has been shown to be asymptotically normal and efficient in Lieberman et al. (2012), but the asymptotic properties of the Whittle ML estimator for these processes have not yet been established in the literature.

5.2 Simulation study: fBm versus fOU

In this section, we evaluate the finite sample performance of the likelihood ratio test in distinguishing between fBm and fOU processes. To generate the data, we use the fOU process (2), with the fractional parameter H set to 0.1, 0.2, or 0.3. The fBm process is generated from (2) with $\kappa = 0$. Under the alternative hypothesis of fOU, we set κ to 1, 5, or 10, representing different levels of local deviations between the fBm and fOU models, where larger values of κ indicate greater dissimilarities. The critical value of the LR test is obtained by bootstrapping, and we set the nominal size of the test to 5%. We perform $1,000$ replications and vary the sample size from $1,000$ to $3,000$ to evaluate the size and power of the LR test.

Table 1: Sizes and powers of the likelihood ratio test: fBm (H_0) versus H_A (fOU). The number of replication is 1000 and the nominal size is 5%.

H	$\kappa = 0$	$\kappa = 1$	$\kappa = 5$	$\kappa = 10$
		$T = 2000$		
0.1	0.051	0.10	0.55	0.60
0.2	0.051	0.12	0.75	0.85
0.3	0.049	0.15	0.87	0.96
		$H = 0.2$		
$T = 1000$	0.051	0.09	0.49	0.77
$T = 2000$	0.051	0.12	0.75	0.85
$T = 3000$	0.051	0.22	0.88	0.94

Table 1 shows the results of the LR test under various parameter configurations. Overall, the LR test performs well in finite samples, with empirical sizes that are close to the nominal size across all settings. As expected, when the difference between the fBm and fOU models is small (i.e., $\kappa = 1$), the test's power is low, reaching only 12% when $T = 2000$ and $H = 0.2$. However, the power increases substantially as the gap between the two models widens. For instance, when $T = 2000$ and $H = 0.2$, the power increases from 12% to 85% as κ increases from 1 to 10. Additionally, we observe that the empirical power of the test increases with larger sample sizes.

6 Financial Volatility Dynamics

Volatility is a critical factor in many financial decisions, and the availability of intraday data allows for the construction of realized volatility measures. In this study, we obtain the daily realized volatility (RV) of several assets, including the S&P 500 index exchange-traded fund (ETF), ETFs tracking various industry indices, and 30 Dow Jones industrial average stocks, from the Risk Lab.[7] The sample period runs from

[7] https://dachxiu.chicagobooth.edu/#risklab.

2012 to 2019. We avoid the subprime mortgage crisis period and the stock turbulence in March 2020 at the onset of Covid-19, as in Shi et al. (2022).

6.1 Model estimation

The logarithm of RV is modeled as the more general process fOU. To estimate the model parameters, we employ three different approaches: AWML, MCL, and CoF. The sampling interval Δ is set to $1/252$ and the parameter μ is taken as the average of the log RV. We use the estimates from CoF as initial values for AWML and MCL. As in our simulations, we set $K = 200$ for AWML. The computing times for MCL and AWML are approximately 20 and 8 seconds, respectively.

Table 2 reports the estimation results of the fOU model for the ten index ETFs (top panel) and the 30 Dow Jones industrial average stocks (bottom panel). The results indicate that AWML and MCL provide very similar estimates for all three model parameters, with the estimated Hurst parameter ranging between 0.12 and 0.23. In contrast, the CoF estimates of H are consistently higher than those of AWML and MCL. The estimated κ of the two maximum likelihood methods falls between 1.5 and 13.23, which implies a very persistent process with the autoregressive coefficient $e^{-\kappa\Delta}$ between 0.95 and 0.994. The CoF estimates of κ and σ^2 are significantly higher than those of the ML methods, suggesting that the former may overestimate the volatility and the degree of mean reversion.

6.2 Likelihood ratio test: fBm versus fOU

While the fOU model is more general, the fBm model is a parsimonious alternative with only one parameter and has been shown to exhibit good forecasting performance (Gatheral et al., 2018). We aim to determine which model is more appropriate for modeling log RV by applying the likelihood ratio tests on the log RVs of the 40 financial assets. We set the null hypothesis of the test to be fBm, and the alternative hypothesis to be fOU.

Figure 5 presents the results of likelihood ratio tests applied to the log RVs of 40 financial assets. The LR test statistics $\widetilde{LR}$ are plotted against their 5% bootstrapped critical values. If the dot is above the horizontal line, it indicates rejection of the null hypothesis of fBm against fOU at a 5% significance level. Evidently, fBm is a suitable model for 21 out of 40 financial assets, while 19 assets are better modeled by fOU. Among the ten ETFs considered, six prefer the fOU model, while four are better modeled by fBm. For the 30 Dow Jones stocks, 13 assets (43%) favor the fOU model, while the fBm null cannot be rejected for the remaining 57% of assets. Overall, the rejection rate across the 40 assets is 47.5%. Interestingly, fBm seems to be a more popular model for individual stocks, while fOU is a preferred choice for index ETFs.

Table 2: Estimation results of fOU for the index ETFs and the 30 Dow Jones Industrial Average stocks

	CoF			MCL			AWML		
	H	κ	σ^2	H	κ	σ^2	H	κ	σ^2
	Index ETFs								
SPY	0.29	11.85	1.64	0.23	5.79	0.91	0.23	4.79	0.90
XLB	0.25	12.08	0.97	0.16	2.41	0.37	0.16	2.17	0.37
XLE	0.34	15.64	1.72	0.19	1.62	0.33	0.20	1.87	0.37
XLF	0.24	15.36	0.97	0.19	7.18	0.54	0.19	5.51	0.53
XLI	0.24	10.73	0.91	0.19	5.32	0.56	0.19	3.67	0.52
XLK	0.26	14.79	1.38	0.21	7.51	0.79	0.20	4.57	0.71
XLP	0.17	4.56	0.42	0.16	4.06	0.40	0.15	2.78	0.36
XLU	0.17	5.22	0.34	0.16	3.56	0.28	0.14	1.56	0.23
XLV	0.22	7.11	0.74	0.19	3.67	0.5	0.18	2.59	0.47
XLY	0.23	9.77	0.93	0.19	4.41	0.56	0.18	3.55	0.55
	Dow Jones 30 stocks								
AAPL	0.36	34.44	3.72	0.21	7.81	0.71	0.21	5.05	0.66
ALD	0.24	18.27	1.04	0.18	7.41	0.52	0.17	4.47	0.46
AMGN	0.22	10.89	0.71	0.15	2.80	0.34	0.15	2.08	0.34
AXP	0.23	23.13	0.96	0.16	7.95	0.42	0.15	5.44	0.38
BA	0.31	32.66	2.23	0.17	6.46	0.50	0.16	2.90	0.43
BEL	0.19	15.70	0.50	0.15	7.84	0.32	0.14	4.62	0.28
CAT	0.26	16.88	1.08	0.14	1.80	0.29	0.13	1.30	0.27
CHV	0.22	4.30	0.52	0.20	2.84	0.41	0.19	1.98	0.37
CRM	0.31	25.50	2.11	0.19	6.06	0.57	0.18	2.68	0.49
CSCO	0.28	21.86	1.16	0.19	6.93	0.44	0.18	3.95	0.39
DIS	0.25	22.61	1.03	0.18	9.08	0.48	0.17	5.52	0.43
GS	0.30	22.57	1.27	0.22	9.59	0.54	0.21	5.90	0.49
HD	0.25	21.32	1.00	0.17	5.93	0.39	0.16	4.45	0.37
IBM	0.29	31.91	1.56	0.17	7.01	0.40	0.16	4.90	0.37
INTC	0.26	17.18	0.91	0.21	9.05	0.53	0.18	3.90	0.40
JNJ	0.12	1.54	0.26	0.14	2.78	0.31	0.13	2.13	0.29
JPM	0.26	15.65	0.98	0.22	8.86	0.60	0.20	5.34	0.52
KO	0.21	12.73	0.58	0.17	6.10	0.36	0.15	3.08	0.29
MCD	0.29	37.41	1.58	0.14	4.75	0.30	0.13	2.62	0.27
MMM	0.26	15.73	1.17	0.17	4.26	0.47	0.16	1.77	0.39
MRK	0.21	15.81	0.66	0.15	5.83	0.35	0.14	3.78	0.32
MSFT	0.29	19.13	1.31	0.21	7.19	0.54	0.21	5.03	0.51
NIKE	0.27	30.84	1.17	0.17	9.78	0.41	0.16	5.47	0.34
PG	0.18	8.02	0.42	0.16	4.99	0.32	0.15	3.54	0.29
SPC	0.17	13.04	0.49	0.12	4.47	0.28	0.12	2.29	0.26
UNH	0.21	14.82	0.68	0.14	4.91	0.35	0.13	2.26	0.29
V	0.23	15.12	0.79	0.16	4.89	0.38	0.15	3.05	0.36
WAG	0.27	37.57	1.67	0.18	13.23	0.57	0.15	5.30	0.43
WMT	0.26	33.99	1.26	0.14	6.32	0.33	0.13	3.53	0.30
XOM	0.25	9.81	0.73	0.19	3.14	0.35	0.18	2.43	0.34

Figure 5: Likelihood ratio tests (H_0 : fBm and H_A : fOU) for log RV of 40 financial assets: 2012 - 2019. The horizon line represents the 5% bootstrapped critical values.

(a) Index ETFs

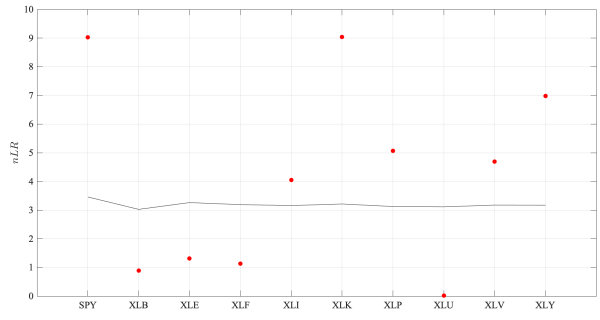

(b) DJ30 stocks

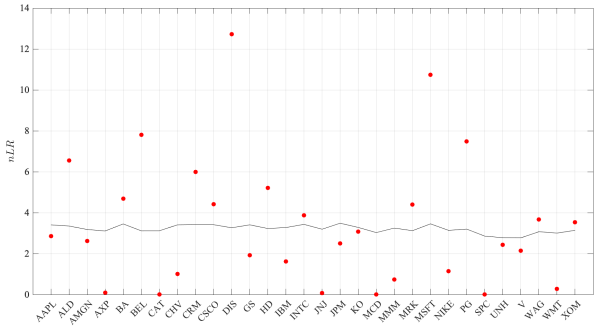

7 Conclusion

Computing the spectral density of the fOU process can be challenging due to an infinite summation in the formula, making it impractical for a widespread use. The commonly used truncation method is inadequate when the Hurst parameter is small, such as 0.1. In this paper, we propose an alternative approach based on the Paxson approximation for the computation of the spectral density. The Paxson approximate spectral density is shown to be not only more accurate but also computationally efficient as compared to the truncation method.

Furthermore, we demonstrate how the Paxson approximate spectral density of fOU can be employed for estimation and hypothesis testing. Specifically, we propose a new approach to estimate parameters of the fOU process using the Paxson approximate spectral density and the Whittle maximum likelihood estimation. Simulation results show that our proposed method outperforms other commonly used methods in the literature. Additionally, we employ the Paxson approximate spectral density to construct a likelihood ratio test to distinguish between the fBm and fOU processes. Simulation results indicate that this test can accurately differentiate between the two processes, particularly when the deviation is moderately large.

We applied both estimation methods and likelihood ratio tests to analyze the log realized volatility of the S&P 500 index ETF, nine industry index ETFs, and 30 Dow Jones industrial average stocks from 2012 to 2019. Our estimated Hurst parameters range from 0.1 to 0.23, indicating rough volatility dynamics. Our testing results are mixed regarding which model, fBm or fOU, is a better fit for the data series. Some data series favor fBm, while others lean towards fOU. Our study adds to the ongoing research on fOU processes and provides new insights into the use of the Paxson approximate spectral density in estimation and hypothesis testing. Additionally, it sheds light on the empirical relevance of fBm and fOU and adds to the literature on rough volatility.

References

Angeletos, G.-M., F. Collard, and H. Dellas (2020). Business-cycle anatomy. *American Economic Review 110*(10), 3030–70. 2

Bayer, C., P. Friz, and J. Gatheral (2016). Pricing under rough volatility. *Quantitative Finance 16*(6), 887–904. 3

Bennedsen, M., K. Christensen, and P. Christensen (2022). Likelihood-based estimation of rough stochastic volatility models. *Working paper*. 2, 10, 11

Beran, J. (1994). *Statistics for Long-Memory Processes*, Volume 61. CRC Press. 14

Bolko, A. E., K. Christensen, M. S. Pakkanen, and B. Veliyev (2022). A GMM approach to estimate the roughness of stochastic volatility. *Journal of Econometrics, forthcoming*. 3

Burnside, C. (1998). Detrending and business cycle facts: A comment. *Journal of Monetary Economics 41*(3), 513–532. 2

Chong, C., M. Hoffmann, Y. Liu, M. Rosenbaum, and G. Szymanski (2022). Statistical inference for rough volatility: Minimax theory. *arXiv preprint arXiv:2210.01214*. 3

Christiano, L. J. and R. J. Vigfusson (2003). Maximum likelihood in the frequency domain: the importance of time-to-plan. *Journal of Monetary Economics 50*(4), 789–815. 2

Dahlhaus, R. (1989). Efficient parameter estimation for self-similar processes. *The Annals of Statistics*, 1749–1766. 10

Fox, R. and M. S. Taqqu (1986). Large-sample properties of parameter estimates for strongly dependent stationary Gaussian time series. *The Annals of Statistics*, 517–532. 9

Fukasawa, M. and T. Takabatake (2019). Asymptotically efficient estimators for self-similar stationary Gaussian noises under high frequency observations. *Bernoulli 25*(3), 1870–1900. 8

Fukasawa, M., T. Takabatake, and R. Westphal (2022). Consistent estimation for fractional stochastic volatility model under high-frequency asymptotics. *Mathematical Finance 32*(4), 1086–1132. 2

Garnier, J. and K. Sølna (2018). Option pricing under fast-varying and rough stochastic volatility. *Annals of Finance 14*(4), 489–516. 4

Gatheral, J., T. Jaisson, and M. Rosenbaum (2018). Volatility is rough. *Quantitative Finance 18*(6), 933–949. 2, 3, 4, 13, 17

Gehringer, J. and X.-M. Li (2020). Functional limit theorems for the fractional ornstein–uhlenbeck process. *Journal of Theoretical Probability*, 1–31. 4

Hu, Y. and D. Nualart (2010). Parameter estimation for fractional ornstein–uhlenbeck processes. *Statistics & Probability Letters 80*(11-12), 1030–1038. 4

Hult, H. (2003). *Topics on fractional Brownian motion and regular variation for stochastic processes*. Ph. D. thesis, Matematik. 4

Lieberman, O., R. Rosemarin, and J. Rousseau (2012). Asymptotic theory for maximum likelihood estimation of the memory parameter in stationary Gaussian processes. *Econometric Theory 28*(2), 457–470. 10, 15

McElroy, T. (2016). Nonnested model comparisons for time series. *Biometrika 103*(4), 905–914. 2, 15

McElroy, T. and A. Roy (2017). Detection of seasonality in the frequency domain. *Statistics*, 01. 2

Messina, J., C. Strozzi, and J. Turunen (2009). Real wages over the business cycle: Oecd evidence from the time and frequency domains. *Journal of Economic Dynamics and Control 33*(6), 1183–1200. 2

Paxson, V. (1997). Fast, approximate synthesis of fractional gaussian noise for generating self-similar network traffic. *ACM SIGCOMM Computer Communication Review 27*(5), 5–18. 2

Samorodnitsky, G. and M. Taqqu (1994). *Stable Non-Gaussian Random Processes*. Chapman & Hall, New York. 25

Shi, S., J. Yu, and C. Zhang (2022). Finite sample comparison of alternative estimators for fractional Gaussian noise. 3, 17

Velasco, C. and P. M. Robinson (2000). Whittle pseudo-maximum likelihood estimation for nonstationary time series. *Journal of the American Statistical Association 95*(452), 1229–1243. 9, 10

Wang, X., W. Xiao, and J. Yu (2023). Modeling and forecasting realized volatility with the fractional Ornstein–Uhlenbeck process. *Journal of Econometrics 234*, 28–52. 2, 3, 10, 13

Wang, X., J. Yu, and C. Zhang (2022). On the optimal forecast with the fractional Brownian motion. *Working paper, Singapore Management University*. 3

Whittle, P. (1951). *Hypothesis testing in time series analysis*, Volume 4. Almqvist & Wiksells boktr. 8

Whittle, P. (1954). On stationary processes in the plane. *Biometrika 41*, 434–449. 2

A Proofs

Proof of Lemma 3.1. (1) Take derivative of $Q(k)$ with respect to k,

$$\frac{\partial Q(k)}{\partial k} = \frac{2\pi(1-2H)(2\pi k-\lambda)^{-2H}\left[(\Delta\kappa)^2+(2\pi k-\lambda)^2\right]-2\pi(2\pi k-\lambda)^{1-2H}2(2\pi k-\lambda)}{\left[(\Delta\kappa)^2+(2\pi k-\lambda)^2\right]^2}.$$

To check the sign of $\partial Q(k)/\partial k$, we can drop the denominator as it is always positive. The numerator of the partial derivative is

$$\begin{aligned}
&2\pi(1-2H)(2\pi k-\lambda)^{-2H}\left[(\Delta\kappa)^2+(2\pi k-\lambda)^2\right]-2\pi(2\pi k-\lambda)^{1-2H}2(2\pi k-\lambda)\\
=&2\pi(2\pi k-\lambda)^{-2H}\left[(1-2H)(\Delta\kappa)^2-(1+2H)(2\pi k-\lambda)^2\right]\\
<&2\pi(2\pi k-\lambda)^{-2H}\left[(\Delta\kappa)^2-(2\pi k-\lambda)^2\right] \text{ since } H>0.
\end{aligned}$$

When $k > \frac{\Delta\kappa+\lambda}{2\pi}$, the first order derivative $\partial Q(k)/\partial k < 0$. For any given value of $\Delta\kappa$, we can always find a K such that for any $k > K$, the function $Q(k)$ is monotone decreasing.

(2) Similarly, the first order derivative of $\tilde{Q}(k)$ is

$$\frac{\partial \tilde{Q}(k)}{\partial k} = \frac{(-2H+1)(\lambda+2\pi k)^{-2H}2\pi[(\Delta\kappa)^2+(\lambda+2\pi k)^2]-(\lambda+2\pi k)^{-2H+1}2(\lambda+2\pi k)2\pi}{\left[(\Delta\kappa)^2+(\lambda+2\pi k)^2\right]^2}.$$

The numerator can be simplified as

$$\begin{aligned}&2\pi(\lambda+2\pi k)^{-2H}[(1-2H)(\Delta\kappa)^2-(1+2H)(\lambda+2\pi k)^2],\\ <&2\pi(\lambda+2\pi k)^{-2H}[(\Delta\kappa)^2-(\lambda+2\pi k)^2], \text{ since } H>0.\end{aligned}$$

It follows that when $k>\frac{\Delta\kappa-\lambda}{2\pi}$, the first order derivative $\partial\tilde{Q}(k)/\partial k<0$. That is, for any given value of $\Delta\kappa$, we can always find a K such that for any $k>K$, the function $Q(k)$ is monotonically decreasing.

(3) From (1) and (2), when $k>\frac{\Delta\kappa+\lambda}{2\pi}$, both $Q(k)$ and $\tilde{Q}(k)$ are monotonically decreasing. Using the properties of harmonic sum, we have

$$\begin{aligned}\int_{K+1}^{\infty}Q(k)\,dk &\leq \sum_{k=K+1}^{\infty}Q(k)\leq\int_{K}^{\infty}Q(k)\,dk,\\ \int_{K+1}^{\infty}\tilde{Q}(k)\,dk &\leq \sum_{k=K+1}^{\infty}\tilde{Q}(k)\leq\int_{K}^{\infty}\tilde{Q}(k)\,dk,\end{aligned}$$

in which left Riemann integrals are the lower bounds and right Riemann integrals are the upper bounds. The upper bounds can be further simplified as

$$\begin{aligned}\int_{K}^{\infty}Q(k)\,dk &= \int_{K}^{\infty}\frac{(2\pi k-\lambda)^{1-2H}}{(\Delta\kappa)^2+(2\pi k-\lambda)^2}dk\\ &\leq \int_{K}^{\infty}(2\pi k-\lambda)^{-1-2H}dk=\frac{1}{4\pi H}(2\pi K-\lambda)^{-2H}\end{aligned}$$

and

$$\begin{aligned}\int_{K}^{\infty}\tilde{Q}(k)\,dk &= \int_{K}^{\infty}\frac{(2\pi k+\lambda)^{1-2H}}{(\Delta\kappa)^2+(2\pi k+\lambda)^2}dk\\ &\leq \int_{K}^{\infty}(2\pi k+\lambda)^{-1-2H}dk=\frac{1}{4\pi H}(2\pi K+\lambda)^{-2H}.\end{aligned}$$

The lower bounds can be further simplified as

$$\begin{aligned}\int_{K+1}^{\infty}Q(k)\,dk &= \int_{K+1}^{\infty}\frac{(2\pi k-\lambda)^{1-2H}}{(\Delta\kappa)^2+(2\pi k-\lambda)^2}dk\\ &= \int_{K+1}^{\infty}\frac{(2\pi k-\lambda)^2}{(\Delta\kappa)^2+(2\pi k-\lambda)^2}\frac{(2\pi k-\lambda)^{1-2H}}{(2\pi k-\lambda)^2}dk\\ &= \int_{K+1}^{\infty}\left[1-\frac{(\Delta\kappa)^2}{(\Delta\kappa)^2+(2\pi k-\lambda)^2}\right]\frac{(2\pi k-\lambda)^{1-2H}}{(2\pi k-\lambda)^2}dk\\ &= \int_{K+1}^{\infty}\frac{(2\pi k-\lambda)^{1-2H}}{(2\pi k-\lambda)^2}dk-\int_{K+1}^{\infty}\frac{(\Delta\kappa)^2}{(\Delta\kappa)^2+(2\pi k-\lambda)^2}\frac{(2\pi k-\lambda)^{1-2H}}{(2\pi k-\lambda)^2}dk\\ &\geq \int_{K+1}^{\infty}(2\pi k-\lambda)^{-1-2H}dk-(\Delta\kappa)^2\int_{K+1}^{\infty}(2\pi k-\lambda)^{-3-2H}dk\end{aligned}$$

$$
\begin{aligned}
&= \frac{1}{4\pi H}\left[2\pi(K+1)-\lambda\right]^{-2H} - (\Delta\kappa)^2 \frac{1}{4\pi(1+H)}\left[2\pi(K+1)-\lambda\right]^{-2-2H} \\
&= \frac{1}{4\pi}\left[2\pi(K+1)-\lambda\right]^{-2H}\left\{\frac{1}{H} - \frac{(\Delta\kappa)^2}{(1+H)\left[2\pi(K+1)-\lambda\right]^2}\right\}
\end{aligned}
$$

and

$$
\begin{aligned}
\int_{K+1}^{\infty} \tilde{Q}(k)\,dk &= \int_{K+1}^{\infty} \frac{(2\pi k+\lambda)^{1-2H}}{(\Delta\kappa)^2+(2\pi k+\lambda)^2}dk \\
&= \int_{K+1}^{\infty} \frac{(2\pi k+\lambda)^2}{(\Delta\kappa)^2+(2\pi k+\lambda)^2}\frac{(2\pi k+\lambda)^{1-2H}}{(2\pi k+\lambda)^2}dk \\
&= \int_{K+1}^{\infty} \left[1-\frac{(\Delta\kappa)^2}{(\Delta\kappa)^2+(2\pi k+\lambda)^2}\right]\frac{(2\pi k+\lambda)^{1-2H}}{(2\pi k+\lambda)^2}dk \\
&\geq \frac{1}{4\pi H}\left[2\pi(K+1)+\lambda\right]^{-2H} - (\Delta\kappa)^2\frac{1}{4\pi(1+H)}\left[2\pi(K+1)+\lambda\right]^{-2-2H} \\
&= \frac{1}{4\pi}\left[2\pi(K+1)+\lambda\right]^{-2H}\left\{\frac{1}{H} - \frac{(\Delta\kappa)^2}{(1+H)\left[2\pi(K+1)+\lambda\right]^2}\right\}
\end{aligned}
$$

Therefore,

$$
\begin{aligned}
\frac{1}{4\pi}\left[2\pi(K+1)-\lambda\right]^{-2H}\left\{\frac{1}{H} - \frac{(\Delta\kappa)^2}{(1+H)\left[2\pi(K+1)-\lambda\right]^2}\right\} &\leq \sum_{x=K+1}^{\infty} Q(k) \leq \frac{1}{4\pi H}(2\pi K-\lambda)^{-2H}, \\
\frac{1}{4\pi}\left[2\pi(K+1)+\lambda\right]^{-2H}\left\{\frac{1}{H} - \frac{(\Delta\kappa)^2}{(1+H)\left[2\pi(K+1)+\lambda\right]^2}\right\} &\leq \sum_{x=K+1}^{\infty} \tilde{Q}(k) \leq \frac{1}{4\pi H}(2\pi K+\lambda)^{-2H}.
\end{aligned}
$$

■

Proof of Theorem 3.1. The discrete time spectral densities of fOU is

$$
f_y^{\Delta}(\lambda) = \frac{\sigma^2}{2\pi} C(H)\Delta^{2H} S(\lambda).
$$

The quantity $S(\lambda)$ can be rewritten as

$$
S(\lambda) = \sum_{k=1}^{K} Q(k) + \sum_{k=K+1}^{\infty} Q(k) + Q_0 + \sum_{k=1}^{K} \tilde{Q}(k) + \sum_{k=K+1}^{\infty} \tilde{Q}(k).
$$

It follows directly from Lemma 3.1(3) ,

$$
S(\lambda) > S_L(\lambda) \equiv \sum_{k=1}^{K} Q(k) + \sum_{k=1}^{K} \tilde{Q}(k) + \frac{\lambda^{1-2H}}{(\Delta\kappa)^2+\lambda^2}
$$

$$+\frac{1}{4\pi}\left[2\pi\left(K+1\right)-\lambda\right]^{-2H}\left\{\frac{1}{H}-\frac{\left(\Delta\kappa\right)^{2}}{\left(1+H\right)\left[2\pi\left(K+1\right)-\lambda\right]^{2}}\right\}$$
$$\frac{1}{4\pi}\left[2\pi\left(K+1\right)+\lambda\right]^{-2H}\left\{\frac{1}{H}-\frac{\left(\Delta\kappa\right)^{2}}{\left(1+H\right)\left[2\pi\left(K+1\right)+\lambda\right]^{2}}\right\}$$

and

$$\begin{aligned} S\left(\lambda\right) &\leq S_{U}\left(\lambda\right)\equiv\sum_{k=1}^{K}Q\left(k\right)+\sum_{k=1}^{K}\tilde{Q}\left(k\right)+\frac{\lambda^{1-2H}}{\left(\Delta\kappa\right)^{2}+\lambda^{2}} \\ &\quad+\frac{1}{4\pi H}\left(2\pi K-\lambda\right)^{-2H}+\frac{1}{4\pi H}\left(2\pi K+\lambda\right)^{-2H} \end{aligned}$$

Therefore, the spectral density $f_{y}^{\Delta}\left(\lambda\right)$ satisfies the following inequality:

$$\frac{\sigma^{2}}{2\pi}C\left(H\right)\Delta^{2H}S_{L}\left(\lambda\right)<f_{y}^{\Delta}\left(\lambda\right)\leq\frac{\sigma^{2}}{2\pi}C\left(H\right)\Delta^{2H}S_{U}\left(\lambda\right). \tag{17}$$

The Paxson approximation of the fOU spectral density is defined as the average of the lower and upper bounds such that

$$\begin{aligned} f_{y}^{\Delta}\left(\lambda\right) &\approx \frac{\sigma^{2}}{2\pi}C\left(H\right)\Delta^{2H}\frac{1}{2}\left[S_{L}\left(\lambda\right)+S_{U}\left(\lambda\right)\right] \\ &= \frac{\sigma^{2}}{2\pi}C\left(H\right)\Delta^{2H}\left\{\sum_{k=1}^{K}Q\left(k\right)+\sum_{k=1}^{K}\tilde{Q}\left(k\right)+\frac{\lambda^{1-2H}}{\left(\Delta\kappa\right)^{2}+\lambda^{2}}\right. \\ &\quad+\frac{1}{8\pi}\left[2\pi\left(K+1\right)-\lambda\right]^{-2H}\left\{\frac{1}{H}-\frac{\left(\Delta\kappa\right)^{2}}{\left(1+H\right)\left[2\pi\left(K+1\right)-\lambda\right]^{2}}\right\} \\ &\quad+\frac{1}{8\pi}\left[2\pi\left(K+1\right)+\lambda\right]^{-2H}\left\{\frac{1}{H}-\frac{\left(\Delta\kappa\right)^{2}}{\left(1+H\right)\left[2\pi\left(K+1\right)+\lambda\right]^{2}}\right\} \\ &\quad\left.+\frac{1}{8\pi H}\left(2\pi K-\lambda\right)^{-2H}+\frac{1}{8\pi H}\left(2\pi K+\lambda\right)^{-2H}\right\}. \end{aligned}$$

■

Proof of Theorem 5.1. Without loss of generality, we assume $\mu=0$ and $y_{0}=0$. Rewrite the fOU process as

$$y_{t}=\int_{-\infty}^{\infty}g_{t}\left(u\right)dB_{u}^{H}\text{ with }g_{t}\left(u\right)=\sigma e^{-\kappa\left(t-u\right)}1_{\left\{u\leq t\right\}},$$

which is the integral on the real line of g with respect to fBm. The first order differenced fOU process (dfOU) is

$$x_{j\Delta}=y_{j\Delta}-y_{\left(j-1\right)\Delta}=\int_{-\infty}^{\infty}\left[g_{j\Delta}\left(u\right)-g_{\left(j-1\right)\Delta}\left(u\right)\right]dB_{u}^{H}.$$

The Fourier transformation of $g_{j\Delta}(u) - g_{(j-1)\Delta}(u)$ is denoted by $\hat{\omega}_{j\Delta}(\lambda)$ and takes the form of

$$\begin{aligned}
\hat{\omega}_{j\Delta}(\lambda) &= \int_{-\infty}^{\infty} e^{iu\lambda} \left[g_{j\Delta}(u) - g_{(j-1)\Delta}(u) \right] du \\
&= \int_{-\infty}^{j\Delta} e^{iu\lambda} \sigma e^{-\kappa(j\Delta - u)} du - \int_{-\infty}^{(j-1)\Delta} e^{iu\lambda} \sigma e^{-\kappa((j-1)\Delta - u)} du \\
&= \sigma \frac{e^{ij\Delta\lambda}}{\kappa + i\lambda} \left(1 - e^{-i\Delta\lambda} \right),
\end{aligned}$$

where λ is the spectral frequency. Since $g_{j\Delta}(u) - g_{(j-1)\Delta}(u)$ belongs to the space of integrands

$$\xi^H = \left\{ \eta(u) : \eta(u) \in L^2(\mathbf{R}), \int_{-\infty}^{\infty} |\hat{\eta}(\lambda)|^2 |\lambda|^{1-2H} d\lambda < \infty \right\}$$

where $\hat{\eta}(\lambda)$ is the Fourier transformation of $\eta(u)$, from Samorodnitsky and Taqqu (1994),

$$\begin{aligned}
E\left(x_{(j+s)\Delta} x_{j\Delta} \right) &= \frac{C(H)}{2\pi} \int_{-\infty}^{\infty} \hat{\omega}_{(j+s)\Delta}(\lambda) \overline{\hat{\omega}_{j\Delta}(\lambda)} |\lambda|^{1-2H} d\lambda \\
&= \sigma^2 \frac{C(H)}{2\pi} \int_{-\infty}^{\infty} \frac{e^{i(j+s)\Delta\lambda}}{\kappa + i\lambda} \frac{e^{-ij\Delta\lambda}}{\kappa - i\lambda} \left| 1 - e^{-i\Delta\lambda} \right|^2 |\lambda|^{1-2H} d\lambda \\
&= \sigma^2 \frac{C(H)}{2\pi} \int_{-\infty}^{\infty} e^{is\Delta\lambda} \left| 1 - e^{-i\Delta\lambda} \right|^2 \frac{|\lambda|^{1-2H}}{\kappa^2 + \lambda^2} d\lambda \\
&= \sigma^2 \frac{C(H)}{2\pi} \sum_{k=-\infty}^{\infty} \int_{(-\pi+2\pi k)/\Delta}^{(\pi+2\pi k)/\Delta} e^{is\Delta\lambda} \left| 1 - e^{-i\Delta\lambda} \right|^2 \frac{|\lambda|^{1-2H}}{\kappa^2 + \lambda^2} d\lambda \\
&= \sigma^2 \frac{C(H)}{2\pi} \Delta^{2H+1} \sum_{k=-\infty}^{\infty} \int_{-\pi}^{\pi} e^{is(\lambda+2\pi k)} \left| 1 - e^{-i(\lambda+2\pi k)} \right|^2 \frac{|\lambda + 2\pi k|^{1-2H}}{(\kappa\Delta)^2 + (\lambda + 2\pi k)^2} d\lambda \\
&= \sigma^2 \frac{C(H)}{2\pi} \Delta^{2H} \sum_{k=-\infty}^{\infty} \int_{-\pi}^{\pi} e^{is\lambda} \left| 1 - e^{-i\lambda} \right|^2 \frac{|\lambda + 2\pi k|^{1-2H}}{(\kappa\Delta)^2 + (\lambda + 2\pi k)^2} d\lambda \\
&= \int_{-\pi}^{\pi} e^{is\lambda} \frac{\sigma^2}{\pi} C(H) (1 - \cos\lambda) \Delta^{2H} \sum_{k=-\infty}^{\infty} \frac{|\lambda + 2\pi k|^{1-2H}}{(\kappa\Delta)^2 + (\lambda + 2\pi k)^2} d\lambda
\end{aligned}$$

since $e^{is2\pi k} = 1$ for any integer s, where $C(H) = \Gamma(2H+1)\sin(\pi H)$. Therefore, the spectral density of $x_{j\Delta}$ is

$$\begin{aligned}
f_x^{\Delta}(\lambda) &= \frac{\sigma^2}{\pi} C(H) (1 - \cos\lambda) \Delta^{2H} \sum_{k=-\infty}^{\infty} \frac{|\lambda + 2\pi k|^{1-2H}}{(\kappa\Delta)^2 + (\lambda + 2\pi k)^2} \\
&= \frac{\sigma^2}{\pi} C(H) (1 - \cos\lambda) \Delta^{2H} S(\lambda).
\end{aligned}$$

Using results from (17), the lower and upper bounds of $f_x^{\Delta}(\lambda)$ are

$$\frac{\sigma^2}{\pi}C(H)(1-\cos\lambda)\Delta^{2H}S_L(\lambda) < f_x^{\Delta}(\lambda) \leq \frac{\sigma^2}{\pi}C(H)(1-\cos\lambda)\Delta^{2H}S_U(\lambda). \tag{18}$$

The Paxson approximation of the dfOU spectral density is

$$\begin{aligned}
f_x^{\Delta}(\lambda) &\approx \frac{\sigma^2}{\pi}C(H)(1-\cos\lambda)\Delta^{2H}\frac{1}{2}\left[S_L(\lambda)+S_U(\lambda)\right] \\
&= \frac{\sigma^2}{\pi}C(H)(1-\cos\lambda)\Delta^{2H}\left\{\sum_{k=1}^{K}Q(k)+\sum_{k=1}^{K}\tilde{Q}(k)+\frac{\lambda^{1-2H}}{(\Delta\kappa)^2+\lambda^2}\right. \\
&\quad +\frac{1}{8\pi}\left[2\pi(K+1)-\lambda\right]^{-2H}\left\{\frac{1}{H}-\frac{(\Delta\kappa)^2}{(1+H)\left[2\pi(K+1)-\lambda\right]^2}\right\} \\
&\quad +\frac{1}{8\pi}\left[2\pi(K+1)+\lambda\right]^{-2H}\left\{\frac{1}{H}-\frac{(\Delta\kappa)^2}{(1+H)\left[2\pi(K+1)+\lambda\right]^2}\right\} \\
&\quad \left.+\frac{1}{8\pi H}(2\pi K-\lambda)^{-2H}+\frac{1}{8\pi H}(2\pi K+\lambda)^{-2H}\right\}.
\end{aligned}$$

■